Journal of Materials Chemistry C

Accepted Manuscript

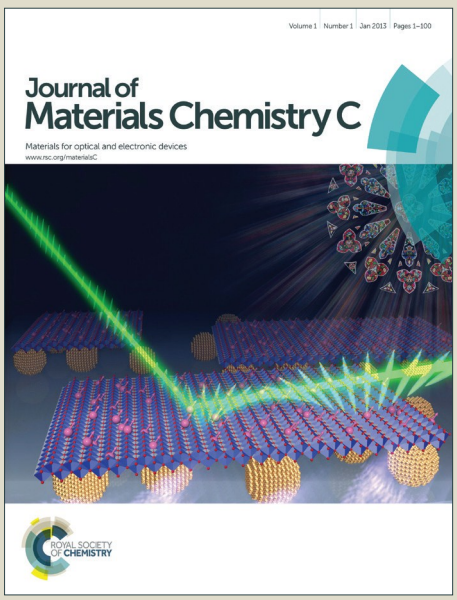

ROYAL SOCIETY OF CHEMISTRY

www.rsc.org/materialsC

Journal Name

RSCPublishing

ARTICLE

Moisture-responsive Films Consisted of Luminescent Polyoxometalate and Agarose†

Cite this: DOI: 10.1039/x0xx00000x

Yun-Feng Qiu,‡[a] Hong Liu,‡[b] Jian-Xun Liu,‡[b] Chen Zhang,[e] Zhuo Ma,[d] Ping-An Hu*[a] and Guang-Gang Gao*[bc],

Received 00th January 2012,
Accepted 00th January 2012

DOI: 10.1039/x0xx00000x

www.rsc.org/

A novel switchable and tunable luminescent composite film consisted of $Na_9[EuW_{10}O_{36}]\cdot 32H_2O$ (EuW_{10}) and agarose has been prepared. EuW_{10} can be converted into non-luminescent species by photoreduction and the recovery is facilitated by oxidation under moisture air. The luminescence recovery of the UV-reduced film showed dependence on the relative humidity (RH) ranging from 43 to 78% in a certain exposure time. X-ray photoelectron energy spectroscopy (XPS) measurements confirm the generation of the reduced W^{5+} species in EuW_{10} polyoxoanion. Further analysis of EuW_{10} indicates that the photo-generated d^1 electron hopping is prohibited in the hybrid film. The absence of recombination of the photogenerated d^1 electrons and holes, and the consumption of holes to form •OH radical are responsible for the luminescence quenching rather than luminescence resonance energy transfer (LRET). The moisture-responsive behavior of EuW_{10}/Agarose film is attributed to the kinetically controlled back reaction of $W^{5+}O_6$ with O_2. Present study provides new insights for lanthanide-containing POMs as tunable luminescent components in UV and moisture dual-responsive materials.

Introduction

Recent development in multifunctional stimuli-responsive systems, such as smart polymer, upconversion luminescence nanomaterials, luminescence complexes, etc., has drawn considerable attention because of their promising applications in smart devices, sensors, environmental monitor, and so on.[1-8] In particular, great efforts have been devoted to the preparation of moisture-responsive materials, which plays important role for the manufacture of sensor system for detecting the concentration of water vapour.[9-11] For instance, most traditional humidity sensors are constructed by monitoring the changes in conductivity or electric constants of ceramic, semiconductor, or polymer upon exposure to varying moisture contents in gas.[12] However, moisture-responsive materials based on electrical properties always require sophisticated measuring equipments and are difficult to construct devices or monitor the readout signals. To facilitate the detection of moisture, development in components acting as chromogenic or fluorogenic sensors to avoid the drawbacks is currently a topic of scientific and technological interest.[13, 14]

Inspired from previous work, europium luminescence or phosphorescence can be quenched by water molecules, which is used to build turn-off sensors with europium based materials. Knall's group developed a detection scheme for moisture using the nonradiative deactivation of the excited state of sensitized europium emission *via* OH-vibrations in the presence of water.[15, 16] In this kind of sensitized europium complexes, the energy transfer from the ligand to the Eu^{3+} ions by the "antenna effect" results the enhanced luminescence of the Eu^{3+} ions.[17] Interestingly, the emission of Eu^{3+} ions can be deactivated obviously. So far, various europium coordination complexes have been synthesized to detect moisture on the basis of this principle. However, the relatively tedious synthetic procedure of ligands and the corresponding photo stability will hinder the development of europium based moisture sensor.

Polyoxometalates (POMs) are widely recognized as active components for constructing smart materials owing to their diverse redox chemistry, electronic, magnetic, photochemical, and catalytic properties.[18-29] In particular, EuW_{10} as one of the most famous fluorescent POMs, is an inorganic cluster containing Eu^{3+} ions, which shows excellent photoluminescent properties with narrow emission bands, large Stokes shift, long lifetime, and long emission timescale.[30-32] Great efforts have been endeavoured to the study of luminescence properties of EuW_{10}, such as luminescence enhancement by complexation,[33] self-healable supramolecular luminescent hydrogels,[30] fluorescence switch,[34] or the improvement of fluorescence lifetime.[35] However, the practical feasibility of these responsive systems was hindered due to the stringent measuring conditions, tedious synthetic purification procedures of polymers, and toxic stimulus. Considering all the aforementioned analysis, EuW_{10} can be reduced by light without causing any structural alteration, but there are no reports on the luminescence quenching caused by photoreduction and related turn-on moisture sensor study. Theoretically, W^{6+} in EuW_{10} can be photoreduced under UV irradiation, and corresponding luminescence properties might be affected, enabling us to

construct smart materials for sensing or biological application based on the monitoring of luminescence.[36] Thus, it is highly appealing to develop a photoreduction strategy to modulate the luminescence of Ln-containing polyoxometalate and recognize the corresponding responsive properties.

Herein, we report for the first time moisture-responsive luminescent EuW_{10}/Agarose composite films using photoreduced EuW_{10} under high energy UV irradiation and/or moisture.

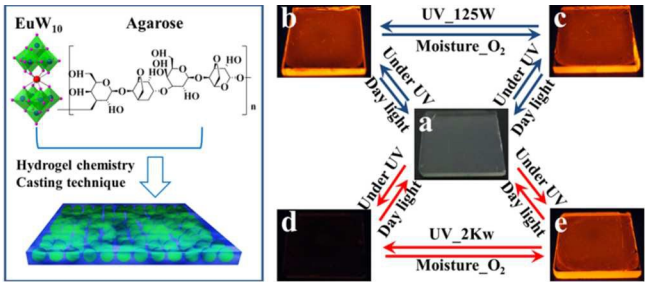

Scheme 1. Schematic illustration of the preparation and images of the moisture-responsive luminescent films. Left panel: the synthetic procedure of composite film by hydrogel assembly. Right panel: (a) 7 *wt*% EuW_{10}@Agarose film on quartz substrate under daylight; (b) Luminescent image of the as-prepared composite film under UV lamp (12 w); (c) 10 min exposure under 125 w UV lamp; (d) 10 min exposure under 2 Kw UV lamp; and (e) recovered film after storing in 78% RH for 10 min. The film size is 1.0 × 1.0 cm.

Experimental section

Materials and methods

All reagents and solvents were commercially available and were used as received. EuW_{10} was synthesized according to previous reference.[37] The structure of EuW_{10} was characterized using UV–vis (**Fig. S1**) and FT-IR (**Fig. S3**). Relative humidity was controlled by salt solution with various concentrations.[38] Ultra-pure Milli-Q water with resistivity of 18.2 MΩ·cm was used for experiments.

UV−vis absorption spectra were collected using Hitachi-4100 UV−vis spectrophotometer (Japan). Luminescence spectra were measured with a Fluoromax-4 spectrometer (Horiba Jobin Yvon) and 265 nm was set as the excitation wavelength for the luminescence measurement of EuW_{10}. FT–IR spectra were collected using Perkin–Elmer 1710 Fourier transform spectrometer with KBr pellets at room temperature. Raman spectra were obtained using Horiba HR800 Raman system with 532 nm excitation. Low laser power was utilized to avoid decomposition of samples. X-ray photoelectron spectroscopy (XPS) analysis was performed on Thermo Scientific K-Alpha XPS using Al (Kα) radiation as the probe. The XPS analysis of the composite films was conducted right after photoreduction in order to avoid oxidation by O_2. Scanning electron microscopy (SEM) measurements were performed on FEI Quanta 200 scanning electron microscope with acceleration voltage of 10 kV. Energy dispersive X-ray spectroscopy (EDS) was coupled with SEM and was measured at 20 kV. The sample was stuck on the observation platform and sprayed with platinum vapour under high vacuum for about 180 s. The characterization of EuW_{10} particles was performed using a field emission transmission electron microscopy (TEM) (TecnaiG2F30, FEI, US).

General procedure for the synthesis of EuW_{10}/agarose composite films. In a typical process, agarose (100 mg) and EuW_{10} (7 mg) powder were added to deionized water (10 mL) at 100°C and stirred vigorously. The cloudy solution mixture became clear after 3 minutes. The films were prepared by drop casting 100 μL solutions on quartz or ITO glass substrates (1 × 1 cm^2). Gelation then took place at room temperature. The composite films were dried after 12 h in air under room temperature, and subsequently peeled off from the ITO substrates.

Results and discussion

Preparation, morphology, and composition analysis

As illustrated in **Scheme 1**, EuW_{10} is difficult to form homogeneous film due to the high surface crystalline energy. Therefore, agarose was selected as matrix to prepare the hybrid composite films with EuW_{10} on the basis of its processability, good miscibility and non-covalent interactions with POMs through abundant –OH groups in agarose skeletons.[39] Considering the basic principle of "heteropolyblue" compounds, agarose can provide proton during the photoreduction of EuW_{10} to form metastable photoreduced complex of agarose and EuW_{10}, which is the prerequisite for our next study. UV-vis and luminescence spectra as a function of EuW_{10} content were shown in **Fig. 1** and **Fig. S1** in the Supporting Information, respectively. Characteristic peak at ca. 258 nm was assigned to ligand-to-metal charge transfer (LMCT) band of O→W in EuW_{10} (Red curve in **Fig. 1**). This peak was also found in the EuW_{10}@Agarose film, confirming successful integration between the two components. As shown in **Fig. 1b**, the characteristic peak of reducible species of EuW_{10} in visible region was not observed due to its low absorption coefficient. Thus, there is no overlap with the emission bands of Eu^{3+} in the visible region. This observation is different from most previous reports on luminescence quenching systems, such as $Eu[(SiW_{10}MoO_{39})_2]^{13-}$ or $[Eu(GeW_{11}O_{39})(H_2O)_2]_2^{10-}$.[39, 40] Seen in **Fig. S1**, the intensities of $^5D_0 \rightarrow {}^7F_1$ and $^5D_0 \rightarrow {}^7F_2$ do not linearly increase due to the fluorescence quenching at higher concentration above 23%. This result is consistent with previous work, in which "concentration quenching" occurs at higher concentrations of $Eu[(SiW_{10}MoO_{39})_2]^{13-}$.[39] In our following study, the composite films with 7 *wt*% EuW_{10} were selected for next investigation.

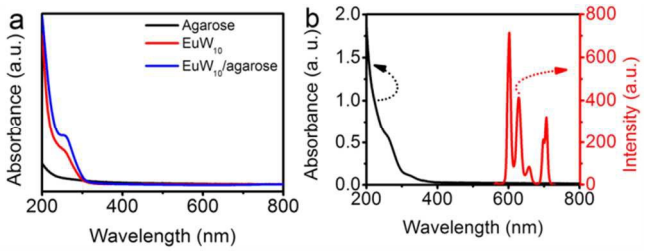

Fig. 1 (a) UV-vis spectra of agarose (black curve), EuW_{10} (red curve), and composite film (blue curve). (b) UV-vis spectrum of composite film after exposure to 2 Kw UV lamp for 10 min (black curve) and luminescence spectrum of as-prepared EuW_{10}/agarose (red curve).

The incorporation of EuW_{10} into the agarose matrix was also confirmed by FTIR and Raman spectra shown in **Fig. S2** and **S3** in the Supporting Information. Based on the structural analysis, the intrinsic interaction between EuW_{10} and agarose was speculated to be hydrogen bonding.[34] As summarized in **Table S1**, four vibrational peaks of EuW_{10} were found at 942 cm^{-1} assigned to ν (W = O_d), 841 cm^{-1} assigned to ν (W-O_b-W), and 781 and 705 cm^{-1} assigned to ν (W-O_c-W). These characteristic peaks were also found in the composite film with slight positional changes. However, the overlap of ν (W = O_d) and the characteristic peak of agarose at ca. 940 cm^{-1} remain unchanged. These results confirmed that EuW_{10} had been successfully incorporated into the agarose matrix and the intact structure of POMs was maintained. The slight position change reveals that there might be strong interactions between EuW_{10} and agarose. Additionally, it is clear that the peak at 3450 cm^{-1} was broadened. A shoulder peak emerged at 3300 cm^{-1}, again indicating strong hydrogen bonding. Raman spectroscopy is a nondestructive characterization technique, providing instructive information for structures. As seen in **Fig. S3**, the bands at 970 and 954 cm^{-1} in EuW_{10} solid powder shifted to 967 and 952 cm^{-1} in composite film, possibly due to the symmetric and asymmetric stretching vibration of the W=O terminal group. When EuW_{10} was incorporated into the film, the 887 cm^{-1} band assigned to W_2–O corner sharing group shifted to 889 cm^{-1}, and the 574 cm^{-1} band assigned to W_3–O corner sharing group shifted to 580 cm^{-1}. These results suggest that the hydrogen bonding between EuW_{10} clusters and polymer skeleton of agarose might cause slight structural distortion of EuW_{10}, and thus the corresponding vibrations also change accordingly.

The as-prepared composite films were optically transparent (**Fig. S4**), and could be peeled off from the substrate to form free-standing films. Shown in **Scheme 1** and **Fig. S5**, the free standing films exhibited red luminescence under UV exposure. SEM images in **Fig. S6** and **Fig. S7** demonstrate the surfaces of the composite films were smooth. EDX spectroscopy mapping analysis of Eu and W elements confirmed even distribution of EuW_{10} in the composite films. From High resolution TEM images shown in **Fig. S8**, black dots of 1.5 ± 0.5 nm in diameter were observed. They were consistent with the size of EuW_{10} clusters. At lower concentration of 7 *wt*%, EuW_{10} clusters distributed uniformly, but some agglomeration region appeared at concentration of 30 *wt*%. This result supports the fluorescence quenching mechanism of "concentration quenching".

Luminescence study

Theoretically, the $W^{5+} \rightarrow W^{6+}$ intervalence charge transfer (IVCT) band of POMs would appear in the visible region after photoreduction. However, **Fig. 1b** clearly showed that there were no new peaks in visible regions after UV irradiation by 125 w (40 mW·cm^{-2}) for 75 min, or 2 kW lamps (120 mW·cm^{-2}) for 10 min. Surprisingly, a new peak at 365 nm (**Fig. S9d**) appeared and was suspected to be due to the supramolecular complex of EuW_{10} and agarose, or LMCT band of $O \rightarrow W^{5+}$. It is noteworthy that the colourless film did not turn into deep blue colour because of the low absorption coefficient in the visible region. In other words, the typical "heteropolyblue" colour from the transition of IVCT was not observed.[41] To our knowledge, the colour of the UV-irradiated POMs depends on the extent of delocalization of the d_1 electron, which was governed by the M–O–M bond angle and reflected the *dπ–pπ–dπ* orbital mixing in the POMs.[36] In most Ln-containing POMs with central heteroatoms or Mo based Keggin structures, d^1 electrons were delocalized due to the existence of corner–shared linkage of M_3O_{13} groups. This allows thermally activated electron-hopping delocalization between corner-shared MO_6 octahedra with M–O–M bond angles of ca. 150°. For instance, the EuSiWMo/agarose composite film was easily reduced to violet colour and generated long-lived and stable charge-separated state due to the favorable *dπ–pπ–dπ* orbital mixing.[39] However, in the structure of EuW_{10} (**Fig. S10**), WO_6 octahedral lattices were edge-shared with W–O–W bond angle of ca. 115°, resulting in the d^1 electron being localized almost only at WO_6 octahedral site due to unfavorable orbital–mixing delocalization.[36] Even though the photochromic process was not clearly observable by naked eyes under daylight, the reduction process could be captured and recorded by monitoring the absorbance change at 365 nm as a function of irradiation time shown in **Fig. S9d**.

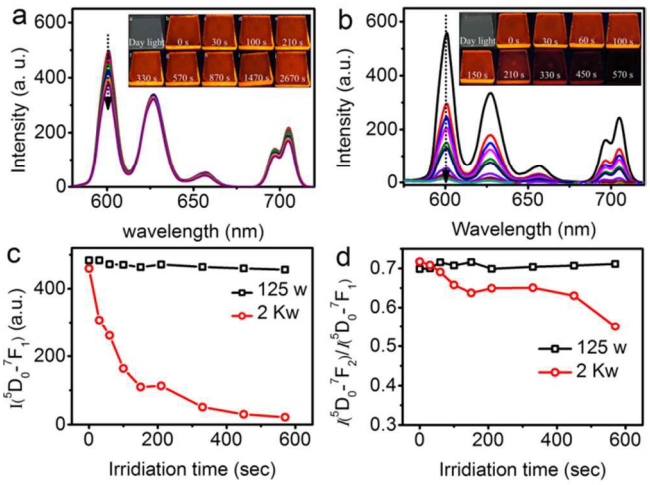

Fig. 2 Comparison of photoreduction process of different UV lamps. (a) and (b) Luminescence spectra of composite films under irradiation by 125 w UV lamp for 75 min and 2 kW UV lamp for 10 min,. (c) $^5D_0 \rightarrow {}^7F_1$ Intensity as a function of irradiation time. (d) Ratio of $I(^5D_0 \rightarrow {}^7F_2)/I(^5D_0 \rightarrow {}^7F_1)$ as a function of irradiation time.

Furthermore, the luminescence of composite film changed considerably as a function of irradiation time as shown in **Fig. 2b**. The initial composite film displayed the characteristic emission of Eu^{3+} at 581 nm ($^5D_0 \rightarrow {}^7F_0$), 601 nm ($^5D_0 \rightarrow {}^7F_1$), 627 nm ($^5D_0 \rightarrow {}^7F_2$), 656 nm ($^5D_0 \rightarrow {}^7F_3$), and 697 and 705 nm ($^5D_0 \rightarrow {}^7F_4$), consistent with those of the solid state EuW_{10}.[33] The intensity of $^5D_0 \rightarrow {}^7F_2$ was attributed to an electric dipole transition and was extremely sensitive to the chemical surroundings in the vicinity of Eu^{3+} ions. The intensity increases as the Eu–O covalency increases and the surrounding environment becomes more symmetrical. However, the intensity of $^5D_0 \rightarrow {}^7F_1$ transition being a magnetic dipole transition is almost independent of the chemical environmental changes of the Eu^{3+}. Shown in **Fig. 2c**, the reduction in luminescence intensity depends on the irradiation time. The intensity of $^5D_0 \rightarrow {}^7F_1$ transition decreased by 5.8% and 23.9% after irradiation by 125 w UV lamp for 10 min and 75 min, respectively. Ratio of $I(^5D_0 \rightarrow {}^7F_2)/I(^5D_0 \rightarrow {}^7F_1)$ was stable with negligible fluctuation as a function of irradiation time, indicative of the unchanged chemical environment of Eu^{3+} ions. However, as shown in **Fig. 2c**, the intensity of $^5D_0 \rightarrow {}^7F_1$ transition drastically decreased by 95.2% after irradiation by 2

Kw UV lamp for 10 min. Meanwhile, the ratio of $I(^5D_0 \rightarrow {}^7F_2)/I(^5D_0 \rightarrow {}^7F_1)$ decreased considerably, indicating a change in the chemical environment of Eu^{3+} ions during the photoreduction process.

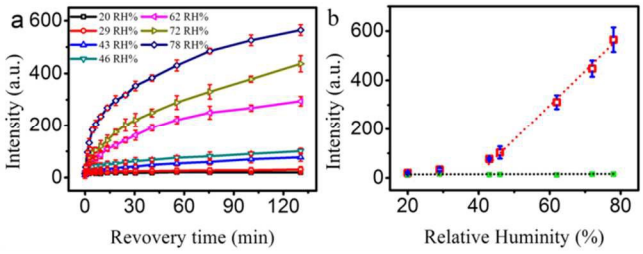

Fig. 3 (a) The $^5D_0 \rightarrow {}^7F_1$ intensity as a function of recovery time under different RH. (b) Plots of the $^5D_0 \rightarrow {}^7F_1$ intensity vs. RH before (black squares) and after (red squares) exposure to various RH for 130 min.

Strikingly, the luminescence recovery of our composite films exhibits intriguing dependence on RH. As shown in **Fig. 3a**, higher RH results in faster recovery rate than that at lower RH. Here, luminescence contrast is defined as the luminescence on/off ratio, i.e. the ratio between the recovered luminescence intensity of the composite film and that of the irradiated composite film. The detection time limit of irradiated film in 43% RH is 18 min, with estimated on/off ratio of 3. As shown in **Fig. 4a**, after aging in 78% RH for 130 min, the luminescence contrast is as high as 37. Meanwhile, the luminescence intensity of composite films after recovery was plotted against RH ranging from 43 to 78% after exposure for 130 min as shown in **Fig. 3b**. A linear relationship was obtained and an empirical equation correlating the intensity (y) and humidity (x) parameters was acquired to be $y = 524.16 + 13.62x$. In addition, the luminescence change of $^5D_0 \rightarrow {}^7F_1$ intensity in composite films under irradiation and aging in 78% RH was reversible as shown in **Fig. 4b**. After seven cycles, the luminescence contrast was still as high as 24, indicating good fatigue property. It should be noted that after longer periods of time (more than 24 hours), the film at lower humidity levels comes up to the value of the 78% RH level. This system really can be used as humidity threshold (lower than 40%) within a shorter period of time (such as 130 min).Therefore, the responsive behavior of the system with high luminescence contrast may potentially pave a new avenue for the practical applications in moisture sensor or information storage.

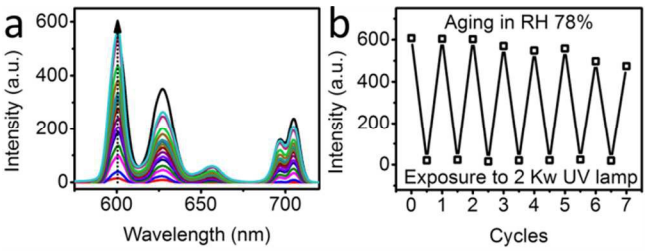

Fig. 4 (a) Luminescence recovery of photoreduced composite film in 78% RH for 130 min. (b) Reversible luminescence changes of $^5D_0 \rightarrow {}^7F_1$ intensity in composite films under irradiation by 2 Kw UV lamp for 10 min and aging in 78% RH for 130 min alternatively.

Because the absorption band of photoreduced EuW_{10} and the emission band of Eu^{3+} in EuW_{10} did not overlap (**Fig. 1b**),[42, 43] LRET as the widely accepted luminescence quenching mechanism might not be suitable to elucidate present case.[39] This unexpected result appeals us to propose a more reasonable explanation for luminescence quenching and moisture-responsive behavior.

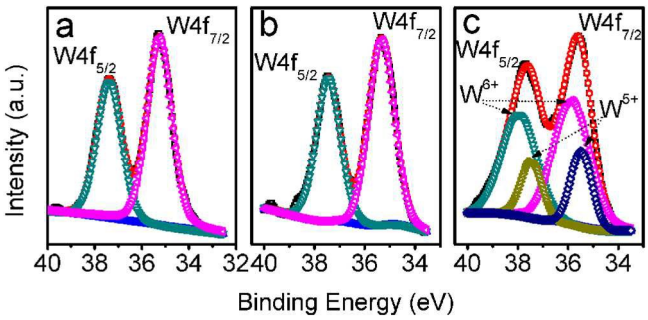

Fig. 5 Deconvoluted XPS spectra of W4f core-level spectra of as-prepared composite films (a), and irradiated films by 125 w (b) and 2 Kw (c) UV lamps for 10 min, respectively.

Luminescence quenching and moisture-responsive mechanism

Generally, the generation of d^1 electrons and holes by photoexcitation of the O→W LMCT bands and the energy transfer to Eu^{3+} in the lattice due to the recombination are two critical processes to luminescence. It is noteworthy that the released energy from the recombination of d^1 electrons and holes is prominent for luminescence. Nevertheless, two things should be emphasized in present system: (1) d^1 electrons were localized almost only at WO_6 octahedral site due to unfavorable orbital–mixing delocalization (W–O–W bond angle is about 115° (**Fig. S10**), whereas favorable angle is ca. 150°), thus the d^1 electron hopping among edge-shared WO_6 was likely forbidden; and (2) the d^1 electron hopping to the Eu^{3+} site was also not allowed due to mismatched orbital–mixing delocalization (Eu–O–W bond angles of about 127°; favorable angle is ca. 150°).[44] Therefore, the dominant contribution for the excitation of Eu^{3+} was likely to be from the radiation energy during the recombination process rather than the electron hopping process.

As shown in **Fig. 5**, XPS analysis was employed to characterize the oxidation state of W species in composite films. All XPS measurements were performed right after irradiation. The W4f core-level spectrum of W atoms in as-prepared composite film could be deconvoluted into the typical spin-orbit doublets. Shown in **Fig. 5a**, the main peaks at 37.9 eV of $W4f_{5/2}$ and 35.8 eV of $W4f_{7/2}$ are attributed to W^{6+}. There is one similar pair of doublet of $W4f_{5/2}$ and $W4f_{7/2}$ for W atoms in the films irradiated by 125 W UV lamp (**Fig. 5b**). For irradiated films by 2 Kw UV lamp shown in **Fig. 5c**, in addition to the characteristic spin-orbit doublet for W^{6+}, the second doublet with lower binding energy at 37.5 eV and 35.5 eV was seen and speculated to be from the emission of $W4f_{5/2}$ and $W4f_{7/2}$ core levels from W^{5+}. The molar percentage of W^{5+} species in irradiated composite films by 2 Kw UV lamp reached ~34.2%. However, it is insufficient to draw the conclusion that there are no W atoms in the 5+ oxidation state in the film irradiated by 125 w UV lamp for longer time. We were unable to capture W^{5+} atoms right after irradiation during XPS measurement because of the

difficulty in setting up in-situ measurements. Thus we tentatively conclude that only 2 Kw UV lamp can provide enough energy to reduce the W atoms in the composite films. Further in-situ measurements are needed to disclose more details about the photoreduction process.

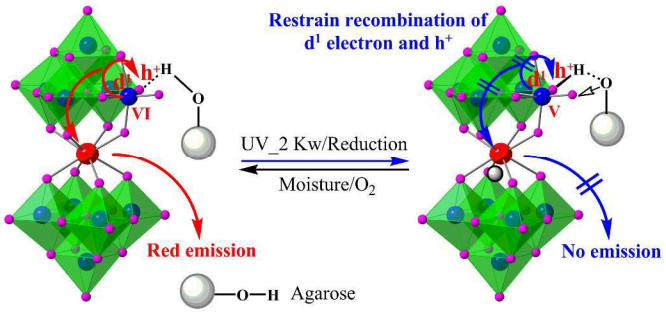

Scheme 2. Proposed luminescence quenching mechanism of composite film. Electron is d^1 and hole is h^+. Blue sphere: W; purple sphere: O.

The proposed luminescence quenching mechanism is illustrated in **Scheme 2**. The transfer of hydrogen from the hydroxyl of agarose to a bridging oxygen atom of EuW_{10} occurs at the photoreduced edge-shared WO_6 octahedral lattice. This is followed by the interaction of d^1 electron with proton which is transferred to the bridging oxygen atom, and further trapped at the $W^{5+}O_6$ sites.[45] Simultaneously, the hole left at the oxygen atom as a result of the O→W LMCT transfer interacts with nonbonding electrons from the oxygen atom of the hydroxyl to generate a metastable charge-separated state. There is also another possibility that the hole interacts with –OH groups from water to form •OH radicals, and this is confirmed by terephthalic acid (TA) photoluminescence probing, a widely applied technique in detecting hydroxyl radical with high sensitivity and selectivity.[46] As shown in **Fig. S11,**[47] TA was non-fluorescent for the composite film without irradiation, whereas the non-luminescent TA was converted to highly fluorescent 2-hydroxy terephthalic acid (HTA) in the presence of the composite film irradiated by 2 Kw UV lamp. As demonstrated in **Fig. S11**, the fluorescence intensity of the solution under irradiation was ~ 32 times higher than that without irradiation. In other words, the charge-separated state and consumption of holes greatly compromised the recombination of d^1 electrons and holes.[36] Without the successful recombination process, the intramolecular energy transfer from O→W LMCT to Eu^{3+} was severely blocked, and hence luminescence was not observed.[34]

When exposed to water moisture, back reaction with O_2 would take place (**Fig. 4a**). This process was triggered by electrons transferred from W^{5+} sites to oxygen molecules. The recovered luminescence intensity was dependent on the rate of back reaction, relating to the swelling properties of agarose films. The concentration of O_2 under all humidity levels in our experiments was around 30%. However, the swelled polymer film under elevated RH would facilitate the mass transfer of oxygen inside the matrix. The increase of the dissolved oxygen concentration inside the films would lead to the acceleration of the back reaction.[48] This assumption was further confirmed by control experiments under N_2 atmosphere at 78% RH, in which the response towards moisture was completely restrained. Based on our experimental results, the back reaction of $W^{5+}O_6$ with O_2 was suspected to be kinetically controlled. The reaction rate constant is triggered by the synergistic effects of O_2 and H_2O, and is greater at higher RH. Thus, the luminescence of composite film was recovered above 43% RH. In comparison, the luminescence recovery was not successful under 20% RH at 25 °C due to the slow reaction rate, consistent with the general theory of reaction rates being temperature dependent. Thermal energy might generate more active molecules, and thus more molecular collisions to accelerate the back reaction. The luminescence contrast of composite film reached 21 under 60 °C in 30 min while other reaction parameters remained unchanged, consistent with previous reported results.[49] Thorough understandings toward the electron-hopping, quenching mechanism, or back reaction variation would need further in-situ experiments or theoretical calculations in future study.

Conclusion

In conclusion, EuW_{10}/agarose composite film was reduced by high energy UV irradiation for the first time and it was responsive to water moisture. The d^1 electrons would be trapped at photoreducible $W^{5+}O_6$ sites, and the holes would leave the hydroxyl oxygen from agarose. The O→W LMCT transfer interacted with nonbonding electrons on the hydroxyl oxygen from agarose, generating a metastable charge-separated state. Blocking the recombination of d^1 electrons and holes, and the consumption of holes to form •OH under photoexcitation were proposed to be responsible for the luminescent quenching instead of LRET, the widely recognized explanation for luminescence quenching in Ln-containing polyoxometalates. The moisture-responsive property of the composite films has been realized taking the advantage of modulating the reaction rate of back reaction. We believe this work will extend the photochemical research on Ln-containing isopolytungstates, which opens up the route for the preparation of luminescent POMs based materials that can find use as UV and moisture dual-responsive applications.

Acknowledgements

We acknowledge supports from the NSFC (Grant No. 21271034 and 21103035), External-Planned Task (No. SKLRS-2013-MS-02) of State Key Laboratory of Robotics and System (HIT), Heilongjiang Universities' Science and Technology Innovation Team program (2012TD010), and China Postdoctoral Science Foundation (No. 20100471047, 2012T50335). We thank Prof. Min Jiang from Qingdao Institute of Bioenergy and Bioprocess Technology, Chinese Academy of Sciences, Prof. Chongshen Guo and Prof. Frueh Johannes from Harbin Institute of Technology for helpful discussions on the XPS analysis and film swelling effect.

Notes and references

[a] State Key Laboratory of Robotics and System (HIT), Harbin, Heilongjiang 150080, China. E–mail: hupa@hit.edu.cn

[b] Department of Chemistry, College of Pharmacy, Jiamusi University, Jiamusi, Heilongjiang, 154007, China. E-mail: gaogg@jmsu.edu.cn

[c] Department of Chemistry, Changchun Normal University, Changchun, 130032, China.

[d] School of Life Science and Technology, Harbin Institute of Technology, 92 West Dazhi Street, Harbin, Heilongjiang, 150001, P.R. China.
[d] Department of Materials Science and Engineering, University of California, Berkeley, CA 94720-1760

† Electronic Supplementary Information (ESI) available: [Experimental data and analysis]. See DOI: 10.1039/b000000x/

‡ These authors made equal contributions to this work.

1. A. P. Blum, J. K. Kammeyer, A. M. Rush, C. E. Callmann, M. E. Hahn and N. C. Gianneschi, *J. Am. Chem. Soc.*, 2015, **137**, 2140-2154.
2. M.-K. Tsang, G. Bai and J. Hao, *Chem. Soc. Rev.*, 2015, **44**, 1585-1607.
3. P. Theato, B. S. Sumerlin, R. K. O'Reilly and T. H. Epps III, *Chem. Soc. Rev.*, 2013, **42**, 7055-7056.
4. L. Isaacs, *Acc. Chem. Res.*, 2014, **47**, 2052-2062.
5. H. Wei, N. Shi, J. Zhang, Y. Guan, J. Zhang and X. Wan, *Chem. Commun.*, 2014, **50**, 9333-9335.
6. P. Guo, G. Zhao, P. Chen, B. Lei, L. Jiang, H. Zhang, W. Hu and M. Liu, *ACS Nano*, 2014, **8**, 3402-3411.
7. X. Chen, L. Mahadevan, A. Driks and O. Sahin, *Nat. Nanotechnol.*, 2014, **9**, 137-141.
8. G. Bai, M.-K. Tsang and J. Hao, *Adv. Opt. Mater.*, 2014, DOI: 10.1002/adom.201400375.
9. D.-D. Han, Y.-L. Zhang, H.-B. Jiang, H. Xia, J. Feng, Q.-D. Chen, H.-L. Xu and H.-B. Sun, *Adv. Mater.*, 2014, DOI: 10.1002/adma.201403587.
10. A. Yamamoto, T. Hamada, I. Hisaki, M. Miyata and N. Tohnai, *Angew. Chem. Int. Ed.*, 2013, **52**, 1709-1712.
11. M. Ma, L. Guo, D. G. Anderson and R. Langer, *Science*, 2013, **339**, 186-189.
12. Z. Chen and C. Lu, *Sensor letters*, 2005, **3**, 274-295.
13. X. Li, X. Gao, W. Shi and H. Ma, *Chem. Rev.*, 2013, **114**, 590-659.
14. L. E. Santos-Figueroa, M. E. Moragues, E. Climent, A. Agostini, R. Martinez-Manez and F. Sancenon, *Chem. Soc. Rev.*, 2013, **42**, 3489-3613.
15. A.-C. Knall, C. Schinagl, A. Pein, N. Noormofidi, R. Saf and C. Slugovc, *Macromol. Chem. Phys.*, 2012, **213**, 2618-2627.
16. A. C. Knall, M. Tscherner, N. Noormofidi, A. Pein, R. Saf, K. Mereiter, V. Ribitsch, F. Stelzer and C. Slugovc, *Analyst*, 2012, **137**, 563-566.
17. L. Song, Y.-W. Wu, W.-X. Chai, Y.-S. Tao, C. Jiang and Q.-H. Wang, *Eur. J. Inorg. Chem.*, 2015, DOI: 10.1002/ejic.201500062.
18. M. T. Pope and A. Müller, *Angew. Chem. Int. Ed.*, 1991, **30**, 34-48.
19. D.-L. Long, E. Burkholder and L. Cronin, *Chem. Soc. Rev.*, 2007, **36**, 105-121.
20. H. Li, S. Pang, S. Wu, X. Feng, K. Müllen and C. Bubeck, *J. Am. Chem. Soc.*, 2011, **133**, 9423-9429.
21. Y.-F. Song, N. McMillan, D.-L. Long, S. Kane, J. Malm, M. O. Riehle, C. P. Pradeep, N. Gadegaard and L. Cronin, *J. Am. Chem. Soc.*, 2009, **131**, 1340-1341.
22. D.-Y. Du, L.-K. Yan, Z.-M. Su, S.-L. Li, Y.-Q. Lan and E.-B. Wang, *Coord. Chem. Rev.*, 2013, **257**, 702-717.
23. Q. Han, C. He, M. Zhao, B. Qi, J. Niu and C. Duan, *J. Am. Chem. Soc.*, 2013, **135**, 10186-10189.
24. S. Omwoma, W. Chen, R. Tsunashima and Y.-F. Song, *Coord. Chem. Rev.*, 2014, **258–259**, 58-71.
25. U. Kortz and T. Liu, *Eur. J. Inorg. Chem.*, 2013, **2013**, 1559-1560.
26. P. Yin, T. Li, R. S. Forgan, C. Lydon, X. Zuo, Z. N. Zheng, B. Lee, D. Long, L. Cronin and T. Liu, *J. Am. Chem. Soc.*, 2013, **135**, 13425-13432.
27. Y. Zhu, P. Yin, F. Xiao, D. Li, E. Bitterlich, Z. Xiao, J. Zhang, J. Hao, T. Liu, Y. Wang and Y. Wei, *J. Am. Chem. Soc.*, 2013, **135**, 17155-17160.
28. P. He, B. Xu, P.-p. Wang, H. Liu and X. Wang, *Adv. Mater.*, 2014, **26**, 4339-4344.
29. L. Huang, S.-S. Wang, J.-W. Zhao, L. Cheng and G.-Y. Yang, *J. Am. Chem. Soc.*, 2014, **136**, 7637-7642.
30. H. Wei, S. Du, Y. Liu, H. Zhao, C. Chen, Z. Li, J. Lin, Y. Zhang, J. Zhang and X. Wan, *Chem. Commun.*, 2014, **50**, 1447-1450.
31. Z. Ma, Q. Liu, Z.-M. Cui, S.-W. Bian and W.-G. Song, *J. Phys. Chem. C*, 2008, **112**, 8875-8880.
32. B. Qin, H. Chen, H. Liang, L. Fu, X. Liu, X. Qiu, S. Liu, R. Song and Z. Tang, *J. Am. Chem. Soc.*, 2010, **132**, 2886-2888.
33. J. Zhang, Y. Liu, Y. Li, H. Zhao and X. Wan, *Angew. Chem. Int. Ed.*, 2012, **51**, 4598-4602.
34. Z. Wang, R. Zhang, Y. Ma, A. Peng, H. Fu and J. Yao, *J. Mater. Chem.*, 2010, **20**, 271-277.
35. J. Xu, S. Zhao, Z. Han, X. Wang and Y.-F. Song, *Chem. Eur. J*, 2011, **17**, 10365-10371.
36. T. Yamase, *Chem. Rev.*, 1998, **98**, 307-326.
37. R. D. Peacock and T. J. R. Weakley, *J. Chem. Soc. A*, 1971, 1836-1839.
38. Q. Kuang, C. Lao, Z. L. Wang, Z. Xie and L. Zheng, *J. Am. Chem. Soc.*, 2007, **129**, 6070-6071.
39. Z. Wang, Y. Ma, R. Zhang, A. Peng, Q. Liao, Z. Cao, H. Fu and J. Yao, *Adv. Mater.*, 2009, **21**, 1737-1741.
40. B. Wang, R.-Q. Meng, L.-H. Bi and L.-X. Wu, *Dalton Trans.*, 2011, **40**, 5298-5301.
41. C. L. Hill, D. A. Bouchard, M. Kadkhodayan, M. M. Williamson, J. A. Schmidt and E. F. Hilinski, *J. Am. Chem. Soc.*, 1988, **110**, 5471-5479.
42. B. Wang, Z.-D. Yin, L.-H. Bi and L.-X. Wu, *Chem. Commun.*, 2010, **46**, 7163-7165.
43. H. Gu, L. Bi, Y. Fu, N. Wang, S. Liu and Z. Tang, *Chem. Sci.*, 2013, **4**, 4371-4377.
44. Y.-Y. Li, F. Gao, J. E. Beves, Y.-Z. Li and J.-L. Zuo, *Chem. Commun.*, 2013, **49**, 3658-3660.
45. M. Jiang and M. Liu, *J. Colloid Interface Sci.*, 2007, **316**, 100-106.
46. A.-L. Hu, Y.-H. Liu, H.-H. Deng, G.-L. Hong, A.-L. Liu, X.-H. Lin, X.-H. Xia and W. Chen, *Biosens. Bioelectron.*, 2014, **61**, 374-378.
47. J. C. Barreto, G.S. Smith, N. H. P. Strobel, P. A. McQuillin and T. A. Miller, *Life Sci.*, 1995, **56**, 89-96.
48. A. Hayashi and T. Kanzaki, *Food Hydrocoll.*, 1987, **1**, 317-325.
49. T. He and J. Yao, *Prog. Mater. Sci.*, 2006, **51**, 810-879.

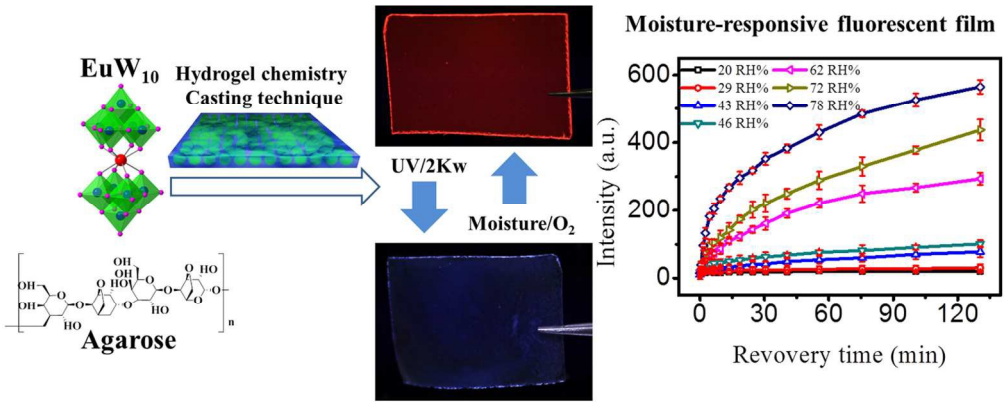

126x50mm (300 x 300 DPI)